catalysts

MDPI

Article

Facile Synthesis of Bi_2MoO_6 Microspheres Decorated by CdS Nanoparticles with Efficient Photocatalytic Removal of Levfloxacin Antibiotic

Shijie Li [1,*], Yanping Liu [2], Yunqian Long [1,*], Liuye Mo [1], Huiqiu Zhang [1] and Jianshe Liu [3]

[1] Key Laboratory of Key Technical Factors in Zhejiang Seafood Health Hazards, Institute of Innovation & Application, Zhejiang Ocean University, Zhoushan 316022, China; liuyemo@zjou.edu.cn (L.M.); zhanghuiqiu2006@163.com (H.Z.)

[2] Department of Environmental Engineering, Zhejiang Ocean University, Zhoushan 316022, China; liuyp@zjou.edu.cn

[3] State Environmental Protection Engineering Center for Pollution Treatment and Control in Textile Industry, College of Environmental Science and Engineering, Donghua University, Shanghai 201620, China; liujianshe@dhu.edu.cn

* Correspondence: lishijie@zjou.edu.cn (S.L.); longyunqian@163.com (Y.L.); Tel.: +86-21-67792557 (S.L.)

Received: 26 September 2018; Accepted: 18 October 2018; Published: 19 October 2018

Abstract: Developing high-efficiency and stable visible-light-driven (VLD) photocatalysts for removal of toxic antibiotics is still a huge challenge at present. Herein, a novel CdS/Bi_2MoO_6 heterojunction with CdS nanoparticles decorated Bi_2MoO_6 microspheres has been obtained by a simple solvothermal-precipitation-calcination method. 1.0CdS/Bi_2MoO_6 has stronger light absorption ability and highest photocatalytic activity with levofloxacin (LEV) degradation efficiency improving 6.2 or 12.6 times compared to pristine CdS or Bi_2MoO_6. CdS/Bi_2MoO_6 is very stable during cycling tests, and no appreciable activity decline and microstructural changes are observed. Results signify that the introduction of CdS could enhance the light absorption ability and dramatically boost the separation of charge carriers, leading to the excellent photocatalytic performance of the heterojunction. This work demonstrates that flower-like CdS/ Bi_2MoO_6 is an excellent photocatalyst for the efficient removal of the LEV antibiotic.

Keywords: CdS; Bi_2MoO_6 microspheres; antibiotic removal; charge separation; visible-light-driven

1. Introduction

Antibiotics accumulated in water have posed a great threat to the environmental safety and human health. In particular, levofloxacin (LEV), as a typical fluoroquinolone antibiotic, has been widely used to treat human and animal infections. As a result, LEV was excessively accumulated in aquatic environments, causing serious health-risk issues by inducing genetic exchange and the bacterial drug resistance [1,2]. Conventional technologies for the removal of antibiotics in aquatic systems have been restricted due to low efficiency, high cost and/or sophisticated instrumentation. In recent years, the semiconductor-based photocatalysis as a green oxidation technology, has made significant developments for treating water pollutions [3–10]. Bismuth (III)-based semiconductors (e.g., BiOX (X = Cl, Br, I) [11–13], Bi_2MoO_6 [14–17], and Bi_2WO_6 [18]) have been emerging as kinds of high-efficiency photocatalysts. Among them, Bi_2MoO_6 as a good visible-light-driven (VLD) photocatalyst, has been one of the focal research points in the area of photocatalysis. Unlike the popular TiO_2, which only can respond to the ultraviolet light, Bi_2MoO_6 (Eg ≈ 2.5–2.8 eV) is active in the visible-light region. However, Bi_2MoO_6 still suffers from the narrow range of sunlight response and fast electron-hole recombination [15–17,19]. Intriguingly, the fabrication of semiconductor heterojunctions

is a crucial way to obtain superior photocatalysts [20]. Thus, a multiple of Bi_2MoO_6-based heterojunctions have been fabricated to ameliorate the photocatalytic activity for the removal of pollutants, such as BN/Bi_2MoO_6 [21], Bi/Bi_2MoO_6 [22], C_3N_4/Bi_2MoO_6 [23,24], TiO_2/Bi_2MoO_6 [25], etc. [26–31]. Our group has also developed some Bi_2MoO_6-based heterojunction photocatalysts with excellent photocatalytic properties [32–36]. However, the majority of them were employed to degrade traditional dyes to evaluate their activity, their application in decomposing colorless and refractory pollutants were underdeveloped.

CdS is known as a promising VLD photocatalyst in virtue of its favorable visible-light-response, and chemical stability [37–40]. Due to the well-matched band structures of CdS and Bi_2MoO_6 [31], it is anticipated the rationally designed CdS/Bi_2MoO_6 can be endowed with superior photocatalytic activity for the removal of LEV antibiotic. However, reports on photocatalytic degradation of LEV antibiotic using flower-like CdS/Bi_2MoO_6 have not been indicated.

Inspired by the above aspects, we designed a flower-like CdS/Bi_2MoO_6 for the removal of the LEV antibiotic. A facile solvothermal-precipitation-calcination method was employed to construct hierarchical CdS/Bi_2MoO_6 heterojunctions with tightly interfacial contact. 1.0CdS/Bi_2MoO_6 possesses the highest activity towards the removal of LEV antibiotic. The plausible photocatalytic mechanism for the degradation of LEV antibiotic over CdS/Bi_2MoO_6 was also illustrated.

2. Results

2.1. Preparation and Characterization

CdS/Bi_2MoO_6 heterojunctions with CdS/Bi_2MoO_6 molar ratios of 0.5:1, 0.75:1, 1.0:1, and 1.5:1 were fabricated and denoted as 0.5CdS/Bi_2MoO_6, 0.75CdS/Bi_2MoO_6, 1.0CdS/Bi_2MoO_6, and 1.5CdS/Bi_2MoO_6, respectively. The crystalline phases of Bi_2MoO_6, CdS, and the optimal sample (1.0CdS/Bi_2MoO_6) were examined by XRD technique (Figure 1). All the diffraction peaks for Bi_2MoO_6 and CdS correspond to crystal planes of orthorhombic (JCPDS 76-2388) [25,33] and (JCPDS 75-1545) [31], respectively. As for 1.0 CdS/Bi_2MoO_6, both the diffraction peaks belonging to Bi_2MoO_6 and CdS were detected in the XRD pattern, verifying the fabrication of CdS/Bi_2MoO_6.

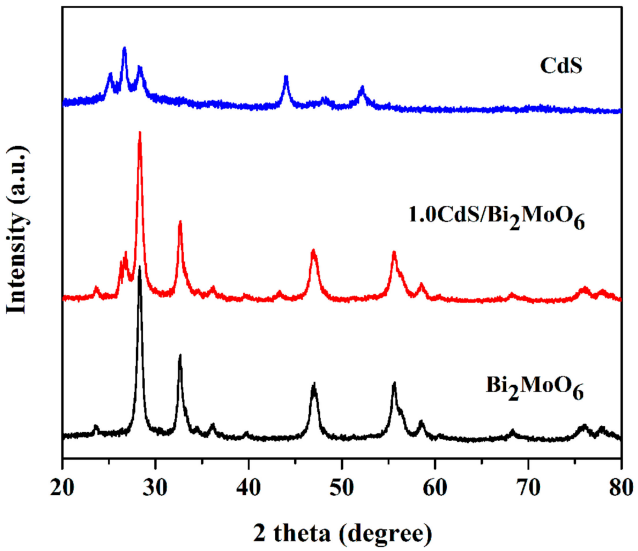

Figure 1. XRD patterns of Bi_2MoO_6, CdS, and 1.0CdS/Bi_2MoO_6.

The morphology of Bi_2MoO_6 and 1.0CdS/Bi_2MoO_6 was characterized by SEM and TEM analysis. As shown in Figure S1, pristine Bi_2MoO_6 has the shape of a microsphere with a smooth surface, in accordance with the morphology of the reported Bi_2MoO_6 [25]. In comparison with Bi_2MoO_6, the surface of 1.0CdS/Bi_2MoO_6 became rough due to the coating of CdS nanoparticles (size: 5–25 nm)

(Figure 2a,b), such a hetero-structure favors the separation of charges. In addition, the EDX spectrum shows the co-existence of Cd, S, Bi, Mo and O elements in 1.0CdS/Bi_2MoO_6 (Figure 2c). The detailed microstructure of 1.0CdS/Bi_2MoO_6 revealed by TEM analysis (Figure 2d) shows that the surfaces of Bi_2MoO_6 nanoplates (size: 200 nm) are deposited by numerous of CdS nanoparticles (size: 5–25 nm). The above characterizations further verify the formation of CdS/Bi_2MoO_6.

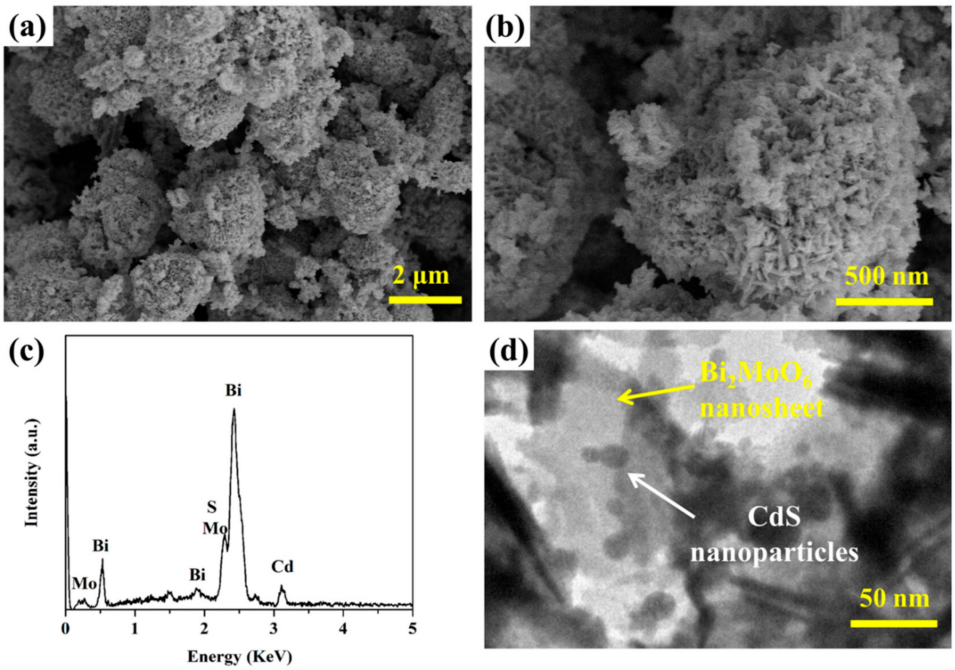

Figure 2. (**a**,**b**) SEM images, (**c**) EDX spectrum, and (**d**) TEM image of 1.0CdS/Bi_2MoO_6.

The UV-Vis absorption spectra of Bi_2MoO_6, CdS, and 1.0CdS/Bi_2MoO_6 are illustrated in Figure 3. Pure Bi_2MoO_6 and CdS exhibit good absorption in the visible light region, consistent with the previous reports [18,37,40]. Notably, 1.0CdS/Bi_2MoO_6 presents better optical absorption than Bi_2MoO_6, indicating that 1.0CdS/Bi_2MoO_6 possesses a better ability to harvest sunlight.

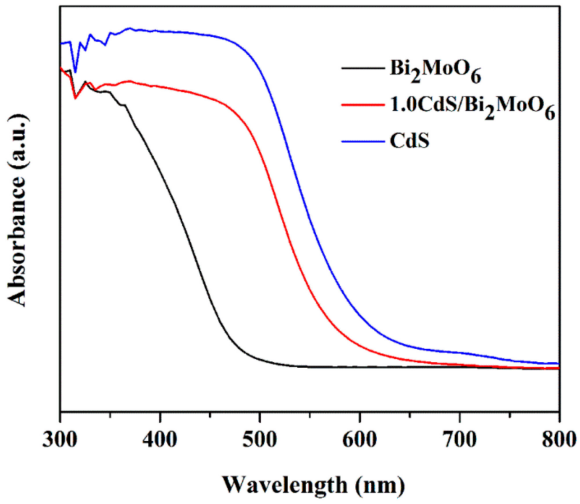

Figure 3. UV-vis absorbance spectra of bare Bi_2MoO_6, CdS, and 1.0CdS/Bi_2MoO_6.

2.2. Photocatalytic Performance

A typical fluoroquinolone antibiotic LEV is a kind of persistent organic pollutants (POPS) due to its water solubility and chemical stability. Photocatalysis is a promising technique for the removal

of LEV antibiotic. For example, Kaur et al. fabricated Bi_2WO_6 nanocuboid (0.75 g/L) for almost 80% degradation of LEV (10 mg/L) within 150 min under visible light irradiation [41]. In this work, the photocatalytic activity of CdS/Bi_2MoO_6 heterojunctions was also evaluated by degrading LEV as a representative toxic antibiotic under visible light (Figure 4). No LEV degradation was detected in the blank test (without catalysts). Pure CdS or Bi_2MoO_6 shows very limited photocatalytic activity, as only 20.6% or 10.8% of LEV was decomposed within 60 min of reaction, owing to the fast recombination of electron-hole pairs. Encouragingly, with the introduction of CdS into the composites, all of the CdS/Bi_2MoO_6 heterojunctions show much enhanced photocatalytic activity compared to pristine CdS and Bi_2MoO_6. Notably, 1.0 CdS/Bi_2MoO_6 obtains the highest activity with 80.4% of LEV degradation within 60 min, much higher than CdS (20.6%), Bi_2MoO_6 (10.9%), or the mechanical mixture (25.8%), verifying the existence of synergistic interaction between CdS and Bi_2MoO_6. Since the introduction of CdS nanoparticles on Bi_2MoO_6 microspheres, the intimately contacted interfacial surface is formed for effective separation of charge carriers. However, with the excessive deposition of CdS (1.5CdS/Bi_2MoO_6), the agglomeration of CdS undermines the synergistic effect, and thus suppresses the interfacial charge transfer, resulting in the decrease of the photocatalytic activity.

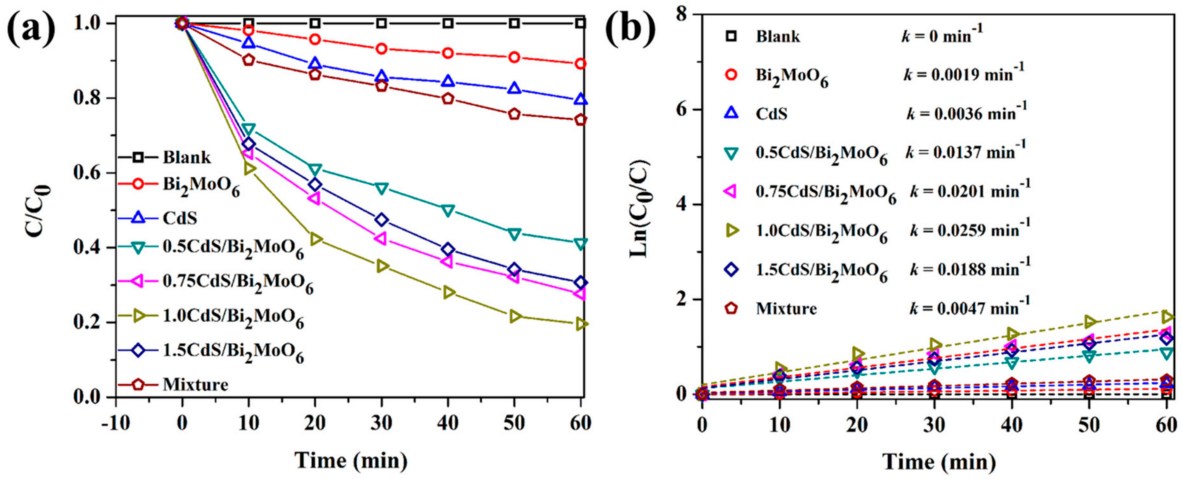

Figure 4. (**a**) The photo-degradation efficiency against LEV (20 mg L^{-1}, 100 mL) by different catalysts (35 mg). (**b**) Kinetic modeling for LEV removal over different catalysts.

To make a quantitative comparison, the LEV degradation data were fitted with the pseudo-first-order model (Figure 4b), $-\ln(C/C_0) = kt$. Clearly, 1.0CdS/Bi_2MoO_6 has the largest rate constant of 0.0259 min^{-1}, which is approximately 6.2, 12.6 or 4.5 times higher than pristine CdS (0.0036 min^{-1}), Bi_2MoO_6 (0.0019 min^{-1}), and the mixture (0.0047 min^{-1}).

The mineralization of organic contaminants is pivotal in the wastewater treatment. To assess the mineralization of LEV, TOC values were recorded during the degradation of LEV (40 mg L^{-1}, 200 mL) by 1.0CdS/Bi_2MoO_6 (200 mg). As depicted in Figure 5, 90.1% of TOC was removed after 2.5 h of reaction. These results indicate that 1.0CdS/Bi_2MoO_6 could effectively decompose and mineralize the LEV antibiotic.

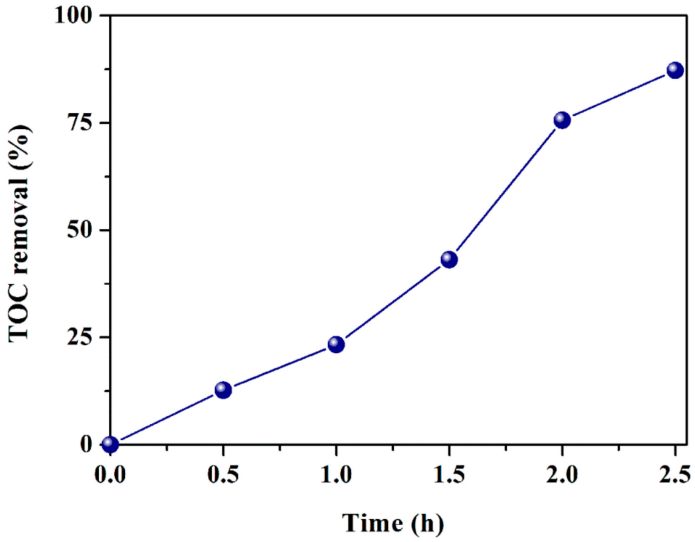

Figure 5. TOC removal profile of LEV (40 mg L^{-1}, 200 mL) over 1.0CdS/Bi_2MoO_6 (200 mg).

The reusability of a photocatalyst is an important factor for the practical treatment of wastewater. Therefore, the cycling runs in LEV degradation over 1.0CdS/Bi_2MoO_6 were executed. Inspiringly, 1.0CdS/Bi_2MoO_6 retained its initial photocatalytic activity after six successive runs (Figure 6a). Moreover, compared to the crystal phase of the fresh 1.0CdS/Bi_2MoO_6, no obvious phase changes (Figure 6b) of the used one was detected, illustrating that 1.0CdS/Bi_2MoO_6 has superior stability and reusability.

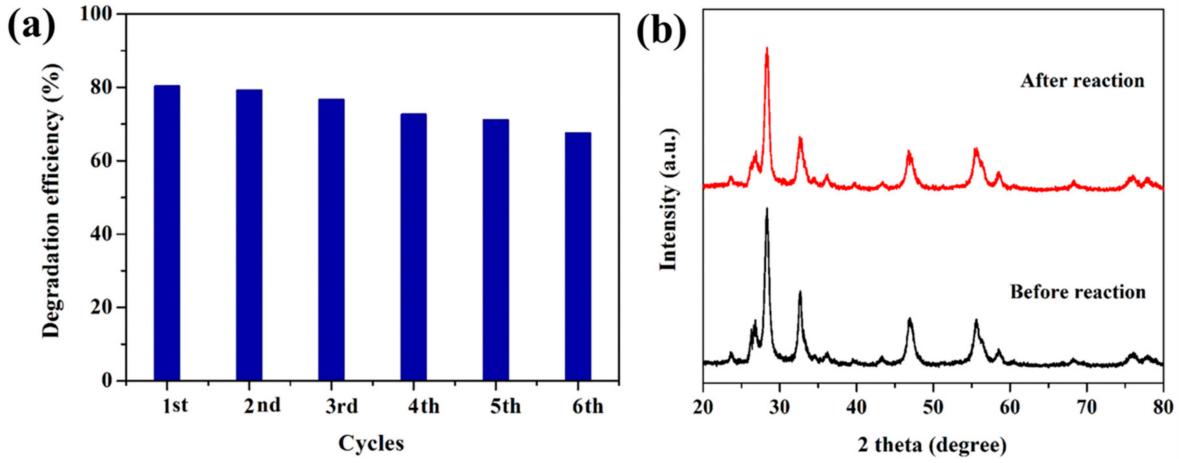

Figure 6. (**a**) Recycling tests of 1.0CdS/Bi_2MoO_6 for LEV degradation; (**b**) XRD patterns of 1.0CdS/Bi_2MoO_6 before and after six cycles.

2.3. Photocatalytic Reaction Mechanism

A batch of experiments was conducted to analyze the photocatalytic reaction mechanism accounting for the degradation of the LEV antibiotic under visible light through adding various scavengers (Figure 7). The LEV degradation rate showed no obvious decline when IPA (scavenger of •OH) was introduced, indicating that •OH did not play a pivotal role. By contrast, the LEV degradation rate was substantially suppressed by BQ (quencher of $O_2^{\bullet-}$) or AO (quencher of h^+), reflecting that $O_2^{\bullet-}$ and h^+ could be the dominant active species responsible for the LEV degradation over 1.0CdS/Bi_2MoO_6.

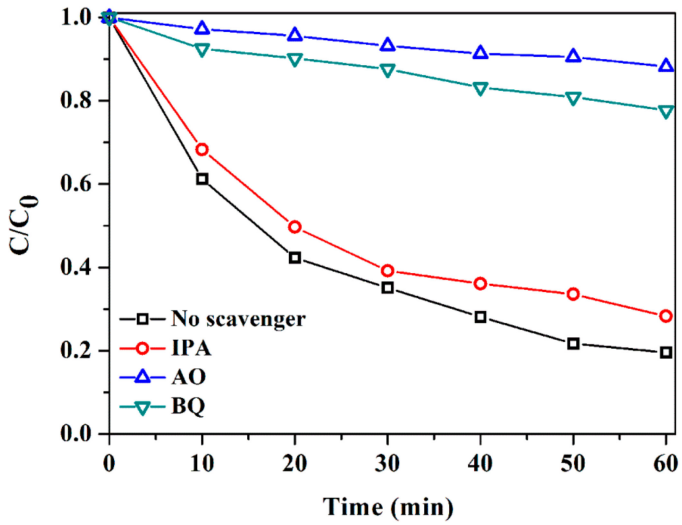

Figure 7. Photo-degradation of LEV (20 mg L^{-1}, 100 mL) by1.0CdS/Bi_2MoO_6 (35 mg) under visible light in the presence of isopropyl alcohol (IPA), ammonium oxalate (AO), and benzoquinone (BQ).

The bandgap (E_g) of Bi_2MoO_6 and CdS were calculated by the equation: $(\alpha h\nu) = A(h\nu\text{-}E_g)^{n/2}$. As presented in Figure S2, the E_g of Bi_2MoO_6 and CdS are about 2.66 eV and 2.24 eV, consistent with the reference [32,40,42]. The valence band (VB) and conduction band (CB) of Bi_2MoO_6 and CdS can be obtained by the following equation: $E_{VB} = X - E_0 + 0.5\,E_g$ (1), $E_{CB} = E_{VB} - E_g$ (2). Thereby, the E_{VB} and E_{CB} of Bi_2MoO_6 were −0.32 and 2.34 eV [36], while those of CdS were −0.56 and 1.68 eV [40]. Apparently, a staggered type II band structure can be constructed in CdS /Bi_2MoO_6, beneficial to retarding the recombination of charge carriers.

Since the separation and transport rate of electron-hole pairs of a semiconductor are closely related to the fluorescence emission [29,43–45], the photoluminescence (PL) technique was applied to study the transport behaviors of charge carriers in Bi_2MoO_6 and 1.0CdS/Bi_2MoO_6 (Figure S3). Through comparing the PL emission spectra of Bi_2MoO_6 and 1.0CdS/Bi_2MoO_6 (Figure S3), it is found that 1.0CdS/Bi_2MoO_6 exhibits much lower fluorescence intensity compared to that of pure Bi_2MoO_6, indicating that the nano-junction between Bi_2MoO_6 and CdS greatly promotes the separation of electron-hole pairs.

On the basis of above experimental results, the interfacial charge transfer behavior of CdS/Bi_2MoO_6 is illustrated in Figure 8. Under visible-light illumination, electron-hole pairs can be produced in both CdS and Bi_2MoO_6. The photo-excited e^- in the CB of CdS may rapidly migrate to that of Bi_2MoO_6, while the photo-excited holes in the VB of Bi_2MoO_6 can preferably drift to that of CdS. Such an interfacial charge movement can effectively retard the electron-hole recombination, accounting for the amelioration of photocatalytic performance of CdS/Bi_2MoO_6. The CB potential of CdS (−0.56 eV) and is Bi_2MoO_6 (−0.32 eV) are more negative than E ($O_2/O_2^{\bullet-}$) (+0.13 eV) [46], thus the e^- in the CB of CdS and Bi_2MoO_6 can react with O_2 to generate active $O_2^{\bullet-}$, further decomposing LEV antibiotic. On the other hand, the holes collected in the VB of CdS and Bi_2MoO_6 can directly decompose the LEV antibiotic due to their strong oxidation ability.

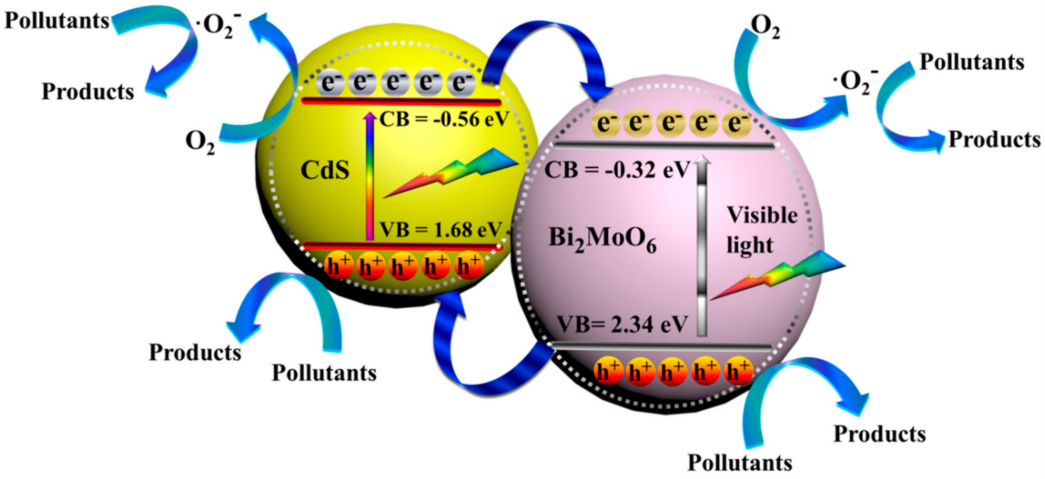

Figure 8. Photocatalytic mechanism scheme over CdS/Bi_2MoO_6.

3. Materials and Methods

3.1. Chemicals

All reagents were purchased from Shanghai Chemical Reagent factory (China) and used directly.

3.2. Chemicals Synthesis of Catalysts

Synthesis of Bi_2MoO_6: Typically, 1 mmol $Bi(NO_3)_3 \cdot 5H_2O$ and 0.5 mmol $Na_2MoO_4 \cdot 2H_2O$ were added into 50 mL of ethylene glycol, and the mixture turned into clear solution with the assistance of ultrasonication for 0.5 h. After that, 30 mL of ethanol was poured into the above solution and kept stirring for 0.5 h. Subsequently, the resulting solution transferred into an autoclave with the volume of 100 mL and reacted at 160 °C for 20 h in an oven.

Synthesis of CdS/Bi_2MoO_6: 0.5 mmol Bi_2MoO_6 was suspended into 50 mL of deionized water. Then, 1mmol $CdCl_2 \cdot 2.5H_2O$ was dissolved in the above suspension under vigorously stirring. After that, 40 mL of Na_2S (1 mmol) aqueous solution was added into the above system dropwise under magnetically stirring for 2 h. The precipitation labeled as 1.0 CdS/Bi_2MoO_6 was washed, dried and then calcined at 200 °C for 2 h in N_2 atmosphere to obtain the catalysts. Through adjusting the amount of precursor of CdS, the samples with CdS/Bi_2MoO_6 molar ratios of 0.5:1, 0.75:1, and 1.5:1 are labeled as $0.5CdS/Bi_2MoO_6$, $0.75CdS/Bi_2MoO_6$, and $1.5CdS/Bi_2MoO_6$, respectively. The CdS sample was also prepared by the same procedure in the absence of Bi_2MoO_6.

3.3. Characterization

The phases of products were characterized via X-ray diffractometer (XRD, Bruker D8 ADVANCE, Karlsruhe, Germany) equipped with mono-chromatized Cu Kα radiation. UV-Vis diffuse reflectance spectra (DRS) of products were collected using Shimadzu UV-2600 spectrophotometer with BaSO4 as the reference standard. Scanning electron microscopy (SEM, Hitachi S-4800, Tokyo, Japan) and transmission electron microscopy (TEM, JEM-2100 JEOL, Tokyo, Japan) were employed to characterize the microstructures of the samples. The corresponding elemental components were analyzed by energy-dispersive X-ray spectroscopy (EDS, Bruker Quantax 400, Berlin, Germany). Photoluminescence (PL) spectra were conducted using Hitachi RF-6000 spectrophotofluorometer with the excitation wavelength of 300 nm.

3.4. Photocatalytic Performance Tests

The photocatalytic property of CdS/Bi_2MoO_6 was assessed by degradation of LEV antibiotic under visible-light illumination, and the light source is provided by a 300 W xenon lamp with a light filter $\lambda > 400$ nm. 50 mg of catalyst was scattered in LEV (100 mL, 20 mg L^{-1}) solution. The suspension

was stirred in the dark for 0.5 h. Then the reaction was initiated when the lamp switches on. During the irradiation, 1.5 mL of suspension was sampled in 10 min. The LEV concentrations were analyzed by using UV-2600 spectrophotometer. Total organic carbon (TOC) of the LEV solutions during reaction was determined by using a Shimadzu TOC analyzer.

4. Conclusions

In summary, CdS nanoparticles interspersed-Bi_2MoO_6 heterojunction photocatalytst was fabricated by a facile solvothermal-precipitation-calcination method. Due to the introduction of CdS, the photo-absorption of CdS/Bi_2MoO_6 and the interfacial charge separation were remarkably enhanced and promoted. By virtue of these benefits, in comparison with bare CdS and Bi_2MoO_6, 1.0CdS/Bi_2MoO_6 presents profoundly enhanced visible-light photocatalytic activity for the removal of the LEV antibiotic. Moreover, 1.0CdS/Bi_2MoO_6 also possesses good stability and can effectively mineralize the LEV antibiotic. This work offers new insight into the design of high-performance Bi-based heterojunction photocatalysts for antibiotic wastewater treatment.

Supplementary Materials: The following are available online at http://www.mdpi.com/2073-4344/8/10/477/s1, Figure S1: SEM image of pure Bi_2MoO_6, Figure S2: The resulting Tauc plots of CdS and Bi_2MoO_6, Figure S3: Photoluminescence (PL) spectra of bare Bi_2MoO_6 and 1.0CdS/Bi_2MoO_6.

Author Contributions: S.L.: idea, and design of the paper; performed the tests; analyzed the data; wrote this paper. Y.L., Y.L., H.Z., L.M., and J.L. assisted the characterizations.

Funding: This work has been financially supported by the National Natural Science Foundation of China (51708504), the Public Projects of Zhejiang Province (LGN18E080003), the Science and Technology Project of Zhoushan (2017C41006), and the Qingdao Science and Technology Program (16-5-1-32-jch).

Conflicts of Interest: The authors declare no conflict of interest.

References

1. Du, J.; Guo, W.; Wang, H.; Yin, R.; Zheng, H.; Feng, X.; Che, D.; Ren, N. Hydroxyl radical dominated degradation of aquatic sulfamethoxazole by Fe^0/bisulfite/O_2: Kinetics, mechanisms, and pathways. *Water Res.* **2018**, *138*, 323–332. [CrossRef]
2. Hong, Y.Z.; Li, C.S.; Zhang, G.Y.; Meng, Y.D.; Yin, B.X.; Zhao, Y.; Shi, W.D. Efficient and stable Nb_2O_5 modified g-C_3N_4 photocatalyst for removal of antibiotic pollutant. *Chem. Eng. J.* **2016**, *299*, 74–84. [CrossRef]
3. Wang, F.; Li, Q.; Xu, D. Recent progress in semiconductor-based nanocomposite photocatalysts for solar-to-chemical energy conversion. *Adv. Energy Mater.* **2017**, *7*, 1700529. [CrossRef]
4. Cates, E.L. Photocatalytic water treatment: So where are we going with this? *Environ. Sci. Technol.* **2017**, *51*, 757–758. [CrossRef] [PubMed]
5. Pirhashemi, M.; Habibi-Yangjeh, A.; Pouran, S.R. Review on the criteria anticipated for the fabrication of highly efficient ZnO-based visible-light-driven photocatalysts. *J. Ind. Eng. Chem.* **2018**, *62*, 1–25. [CrossRef]
6. Zhu, S.S.; Wang, D.W. Photocatalysis: Basic principles, diverse forms of implementations and emerging scientifc opportunities. *Adv. Energy Mater.* **2017**, *7*, 1700841. [CrossRef]
7. Li, S.; Hu, S.; Jiang, W.; Liu, Y.; Liu, Y.; Zhou, Y.; Mo, L.; Liu, J. Ag_3VO_4 nanoparticles decorated $Bi_2O_2CO_3$ micro-flowers: An efficient visible-light-driven photocatalyst for the removal of toxic contaminants. *Front. Chem.* **2018**, *6*, 255. [CrossRef] [PubMed]
8. Li, S.; Hu, S.; Jiang, W.; Liu, Y.; Liu, J.; Wang, Z. Facile synthesis of flower-like Ag_3VO_4/Bi_2WO_6 heterojunction with enhanced visible-light photocatalytic activity. *J. Colloid Interface Sci.* **2017**, *501*, 156–163. [CrossRef] [PubMed]
9. Wang, Y.; Wang, H.; Xu, A.; Song, Z. Facile synthesis of Ag_3PO_4 modified with GQDs composites with enhanced visible-light photocatalytic activity. *J. Mater. Sci. Mater. Electron.* **2018**, *29*, 16691–16701. [CrossRef]
10. Zheng, J.; Chang, F.; Jiao, M.; Xu, Q.; Deng, B.; Hu, X. A visible-light-driven heterojuncted composite WO_3/$Bi_{12}O_{17}Cl_2$: Synthesis, characterization, and improved photocatalytic performance. *J. Colloid Interface Sci.* **2018**, *510*, 20–31. [CrossRef] [PubMed]
11. Cheng, H.F.; Huang, B.B.; Dai, Y. Engineering BiOX (X = Cl, Br, I) nanostructures for highly efficient photocatalytic applications. *Nanoscale* **2014**, *6*, 2009–2026. [CrossRef] [PubMed]

12. Yang, Y.; Zhang, C.; Lai, C.; Zeng, G.; Huang, D.; Cheng, M.; Wang, J.; Chen, F.; Zhou, C.; Xiong, W. BiOX (X = Cl, Br, I) photocatalytic nanomaterials: Applications for fuels and environmental management. *Adv. Colloid Interface Sci.* **2018**, *254*, 76–93. [CrossRef] [PubMed]
13. Li, S.J.; Hu, S.W.; Xu, K.B.; Jiang, W.; Liu, J.S.; Wang, Z.H. A novel heterostructure of BiOI nanosheets anchored onto MWCNTs with excellent visible-light photocatalytic activity. *Nanomaterials* **2017**, *7*, 22–34. [CrossRef] [PubMed]
14. Yu, C.; Wu, Z.; Liu, R.; Dionysiou, D.D.; Yang, K.; Wang, C.; Liu, H. Novel fluorinated Bi_2MoO_6 nanocrystals for efficient photocatalytic removal of water organic pollutants under different light source illumination. *Appl. Catal. B* **2017**, *209*, 1–11. [CrossRef]
15. Jia, Y.; Ma, Y.; Tang, J.; Shi, W. Hierarchical nanosheet-based Bi_2MoO_6 microboxes for efficient photocatalytic performance. *Dalton Trans.* **2018**, *47*, 5542–5547. [CrossRef] [PubMed]
16. Chen, Y.; Yang, W.; Gao, S.; Zhu, L.; Sun, C.; Li, Q. Internal polarization modulation in Bi_2MoO_6 for photocatalytic performance enhancement under visible light illumination. *ChemSusChem* **2018**, *11*, 1521–1532. [CrossRef] [PubMed]
17. Long, J.L.; Wang, S.C.; Chang, H.J.; Zhao, B.Z.; Liu, B.T.; Zhou, Y.G.; Wei, W.; Wang, X.X.; Huang, L.; Huang, W. Bi_2MoO_6 nanobelts for crystal facet-enhanced photocatalysis. *Small* **2014**, *10*, 2791–2795. [CrossRef] [PubMed]
18. Wang, J.; Tang, L.; Zeng, G.; Liu, Y.; Zhou, Y.; Deng, Y.; Wang, J.; Peng, B. Plasmonic Bi metal deposition and g-C_3N_4 coating on Bi_2WO_6 microspheres for efficient visible-light photocatalysis. *ACS Sustain. Chem. Eng.* **2017**, *5*, 1062–1072. [CrossRef]
19. Guo, C.; Xu, J.; Wang, S.; Li, L.; Zhang, Y.; Li, X. Facile synthesis and photocatalytic application of hierarchical mesoporous Bi_2MoO_6 nanosheet-based microspheres. *CrystEngComm* **2012**, *14*, 3602–3608. [CrossRef]
20. Ye, R.; Zhao, J.; Wickemeyer, B.B.; Toste, F.D.; Somorjai, G.A. Foundations and strategies of the construction of hybrid catalysts for optimized performances. *Nat. Catal.* **2018**, *1*, 318–325. [CrossRef]
21. Ke, J.; Duan, X.; Luo, S.; Zhang, H.; Sun, H.; Liu, J.; Tade, M.; Wang, S. UV-assisted construction of 3D hierarchical rGO/Bi_2MoO_6 composites for enhanced photocatalytic water oxidation. *Chem. Eng. J.* **2017**, *313*, 1447–1453. [CrossRef]
22. Zhao, Z.W.; Zhang, W.; Sun, Y.J.; Yu, J.Y.; Zhang, Y.X.; Wang, H.; Dong, F.; Wu, Z.B. Bi cocatalyst/Bi_2MoO_6 microspheres nanohybrid with SPR-promoted visible-light photocatalysis. *J. Phys. Chem. C* **2016**, *120*, 11889–11898. [CrossRef]
23. Opoku, F.; Govender, K.; Sittert, C.G.C.E.V.; Govender, P. Insights into the photocatalytic mechanism of mediator-free direct Z-scheme g-C_3N_4/Bi_2MoO_6 (010) and g-C_3N_4/Bi_2WO_6 (010) heterostructures: A hybrid density functional theory study. *Appl. Surf. Sci.* **2018**, *427*, 487–498. [CrossRef]
24. Ma, T.J.; Wu, J.; Mi, Y.D.; Chen, Q.H.; Ma, D.; Chai, C. Novel Z-Scheme g-C_3N_4/C@Bi_2MoO_6 composite with enhanced visible-light photocatalytic activity for naphthol degradation. *Sep. Purif. Technol.* **2017**, *183*, 54–65. [CrossRef]
25. Zhang, M.Y.; Shao, C.L.; Mu, J.B.; Zhang, Z.Y.; Guo, Z.C.; Zhang, P.; Liu, Y.C. One-dimensional Bi_2MoO_6/TiO_2 hierarchical heterostructures with enhanced photocatalytic activity. *CrystEngComm* **2012**, *14*, 605–612. [CrossRef]
26. Lv, J.; Zhang, J.; Liu, J.; Li, Z.; Dai, K.; Liang, C. Bi SPR-promoted Z-scheme Bi_2MoO_6/CdS-diethylenetriamine composite with effectively enhanced visible light photocatalytic hydrogen evolution activity and stability. *ACS Sustain. Chem. Eng.* **2018**, *6*, 696–706. [CrossRef]
27. Meng, Q.Q.; Zhou, Y.S.; Chen, G.; Hu, Y.D.; Lv, C.; Qiang, L.S.; Xing, W.N. Integrating both homojunction and heterojunction in QDs self-decorated Bi_2MoO_6/BCN composites to achieve an efficient photocatalyst for Cr(VI) reduction. *Chem. Eng. J.* **2018**, *334*, 334–343. [CrossRef]
28. Li, X.; Su, M.; Zhu, G.; Zhang, K.; Zhang, X.; Fan, J. Fabrication of a novel few-layer WS_2/Bi_2MoO_6 plate-on-plate heterojunction structure with enhanced visible-light photocatalytic activity. *Dalton Trans.* **2018**, *47*, 10046–10056. [CrossRef] [PubMed]
29. Zhang, J.L.; Ma, Z. Flower-like Ag_2MoO_4/Bi_2MoO_6 heterojunctions with enhanced photocatalytic activity under visible light irradiation. *J. Taiwan Inst. Chem. Eng.* **2017**, *71*, 156–164. [CrossRef]
30. Zhang, J.L.; Zhang, L.S.; Yu, N.; Xu, K.B.; Li, S.J.; Wang, H.L.; Liu, J.S. Flower-like Bi_2S_3/Bi_2MoO_6 heterojunction superstructures with enhanced visible-light-driven photocatalytic activity. *RSC Adv.* **2015**, *5*, 75081–75088. [CrossRef]

31. Feng, Y.; Yan, X.; Liu, C.; Hong, Y.; Zhu, L.; Zhou, M.; Shi, W. Hydrothermal synthesis of CdS/Bi2MoO6 heterojunction photocatalysts with excellent visible-light-driven photocatalytic performance. *Appl. Surf. Sci.* **2015**, *353*, 87–94. [CrossRef]
32. Li, S.; Jiang, W.; Hu, S.; Liu, Y.; Liu, Y.; Xu, K.; Liu, J. Hierarchical heterostructure of Bi_2MoO_6 micro-flowers decorated with Ag_2CO_3 nanoparticles for efficient visible-light-driven photocatalytic removal of toxic pollutants. *Beilstein J. Nanotechnol.* **2018**, *9*, 2297–2305. [CrossRef] [PubMed]
33. Li, S.; Hu, S.; Jiang, W.; Zhou, Y.; Liu, J.; Wang, Z. Facile synthesis of cerium oxide nanoparticles decorated flower-like bismuth molybdate for enhanced photocatalytic activity toward organic pollutant degradation. *J. Colloid Interface Sci.* **2018**, *530*, 171–178. [CrossRef] [PubMed]
34. Li, S.; Hu, S.; Jiang, W.; Liu, Y.; Zhou, Y.; Liu, Y.; Mo, L. Hierarchical architectures of bismuth molybdate nanosheets onto nickel titanate nanofibers: Facile synthesis and efficient photocatalytic removal of tetracycline hydrochloride. *J. Colloid Interface Sci.* **2018**, *521*, 42–49. [CrossRef] [PubMed]
35. Li, S.; Hu, S.; Zhang, J.; Jiang, W.; Liu, J. Facile synthesis of Fe_2O_3 nanoparticles anchored on Bi_2MoO_6 microflowers with improved visible light photocatalytic activity. *J. Colloid Interface Sci.* **2017**, *497*, 93–101. [CrossRef] [PubMed]
36. Li, S.; Shen, X.; Liu, J.; Zhang, L. Synthesis of Ta_3N_5/Bi_2MoO_6 core-shell fiber-shaped heterojunctions as efficient and easily recyclable photocatalysts. *Environ. Sci. Nano* **2017**, *4*, 1155–1167. [CrossRef]
37. Korala, L.; Germain, J.R.; Chen, E.; Pala, I.R.; Li, D.; Brock, S.L. CdS aerogels as efficient photocatalysts for degradation of organic dyes under visible light irradiation. *Inorg. Chem. Front.* **2017**, *4*, 1451–1457. [CrossRef] [PubMed]
38. Zhang, Y.; Han, L.; Wang, C.; Wang, W.; Ling, T.; Yang, J.; Dong, C.; Lin, F.; Du, X.-W. Zinc-Blende CdS Nanocubes with Coordinated Facets for Photocatalytic Water Splitting. *ACS Catal.* **2017**, *7*, 1470–1477. [CrossRef]
39. Zhao, N.; Peng, J.; Liu, G.; Zhai, M. PVP-capped CdS nanopopcorns with type-II homojunctions for highly efficient visible-light-driven organic pollutant degradation and hydrogen evolution. *J. Mater. Chem. A* **2018**. [CrossRef]
40. Kandi, D.; Martha, S.; Thirumurugan, A.; Parida, K.M. Modification of BiOI microplates with CdS QDs for enhancing stability, optical property, electronic behavior toward rhodamine B decolorization, and photocatalytic hydrogen evolution. *J. Phys. Chem. C* **2017**, *121*, 4834–4849. [CrossRef]
41. Kaur, A.; Kansal, S.K. Bi_2WO_6 nanocuboids: An efficient visible light active photocatalyst for the degradation of levofloxacin drug in aqueous phase. *Chem. Eng. J.* **2016**, *302*, 194–203. [CrossRef]
42. Yang, X.; Xiang, Y.; Wang, X.; Li, S.; Chen, H.; Xing, D. Pyrene-based conjugated polymer/Bi_2MoO_6 Z-scheme hybrids: Facile construction and sustainable enhanced photocatalytic performance in ciprofloxacin and Cr(VI) removal under visible light irradiation. *Catalysts* **2018**, *8*, 185. [CrossRef]
43. Li, S.; Hu, S.; Jiang, W.; Liu, Y.; Liu, J.; Wang, Z. Synthesis of n-type TaON microspheres decorated by p-type Ag_2O with enhanced visible light photocatalytic activity. *Mol. Catal.* **2017**, *435*, 135–143. [CrossRef]
44. Chang, F.; Wu, F.; Zheng, J.; Cheng, W.; Yan, W.; Deng, B.; Hu, X. In-situ establishment of binary composites a-$Fe_2O_3/Bi_{12}O_{17}Cl_2$ with both photocatalytic and photo-Fenton features. *Chemosphere* **2018**, *210*, 257–266. [CrossRef] [PubMed]
45. Li, S.; Jiang, W.; Xu, K.; Hu, S.; Liu, Y.; Zhou, Y.; Liu, J. Synthesis of flower-like AgI/BiOCOOH pn heterojunctions with enhanced visible-light photocatalytic performance for the removal of toxic pollutants. *Front. Chem.* **2018**, *6*, 518.
46. Chen, Y.J.; Tian, G.H.; Shi, Y.H.; Xiao, Y.T.; Fu, H.G. Hierarchical MoS_2/Bi_2MoO_6 composites with synergistic effect for enhanced visible photocatalytic activity. *Appl. Catal. B* **2015**, *164*, 40–47. [CrossRef]